nature genetics

A recurrent *de novo* mutation in *KCNC1* causes progressive myoclonus epilepsy

Mikko Muona[1–4], Samuel F Berkovic[5], Leanne M Dibbens[6], Karen L Oliver[5], Snezana Maljevic[7], Marta A Bayly[6], Tarja Joensuu[2–4], Laura Canafoglia[8], Silvana Franceschetti[8], Roberto Michelucci[9], Salla Markkinen[2–4], Sarah E Heron[6], Michael S Hildebrand[5], Eva Andermann[10], Frederick Andermann[10], Antonio Gambardella[11], Paolo Tinuper[9,12], Laura Licchetta[9,12], Ingrid E Scheffer[5,13,14], Chiara Criscuolo[15], Alessandro Filla[15], Edoardo Ferlazzo[16,17], Jamil Ahmad[18], Adeel Ahmad[19], Betul Baykan[20,21], Edith Said[22,23], Meral Topcu[24], Patrizia Riguzzi[9], Mary D King[25,26], Cigdem Ozkara[27], Danielle M Andrade[28], Bernt A Engelsen[29,30], Arielle Crespel[31], Matthias Lindenau[32], Ebba Lohmann[32–34], Veronica Saletti[35], João Massano[36,37], Michael Privitera[38], Alberto J Espay[39], Birgit Kauffmann[40], Michael Duchowny[41,42], Rikke S Møller[43,44], Rachel Straussberg[45,46], Zaid Afawi[46,47], Bruria Ben-Zeev[46,48], Kaitlin E Samocha[49–52], Mark J Daly[49–51], Steven Petrou[13,53], Holger Lerche[7], Aarno Palotie[1,49–51,54–56] & Anna-Elina Lehesjoki[2–4]

Progressive myoclonus epilepsies (PMEs) are a group of rare, inherited disorders manifesting with action myoclonus, tonic-clonic seizures and ataxia. We sequenced the exomes of 84 unrelated individuals with PME of unknown cause and molecularly solved 26 cases (31%). Remarkably, a recurrent *de novo* mutation, c.959G>A (p.Arg320His), in *KCNC1* was identified as a new major cause for PME. Eleven unrelated exome-sequenced (13%) and two affected individuals in a secondary cohort (7%) had this mutation. *KCNC1* encodes $K_V3.1$, a subunit of the K_V3 voltage-gated potassium ion channels, which are major determinants of high-frequency neuronal firing. Functional analysis of the Arg320His mutant channel showed a dominant-negative loss-of-function effect. Ten cases had pathogenic mutations in known PME-associated genes (*NEU1*, *NHLRC1*, *AFG3L2*, *EPM2A*, *CLN6* and *SERPINI1*). Identification of mutations in *PRNP*, *SACS* and *TBC1D24* expand their phenotypic spectra to PME. These findings provide insights into the molecular genetic basis of PME and show the role of *de novo* mutations in this disease entity.

PMEs are among the most devastating forms of epilepsy. They are clinically and genetically heterogeneous, characterized by core features of action myoclonus, tonic-clonic seizures and progressive neurological decline[1]. Most molecularly characterized PMEs are inherited in an autosomal recessive manner, with rare cases showing autosomal dominant or mitochondrial inheritance[2,3]. Unverricht-Lundborg disease (ULD; MIM 254800) is the most common form of PME in most patient series, and an important clinical feature is the preservation of cognition[1–3]. ULD is caused by mutations in *CSTB*[4], and recently discovered mutations in genes including *SCARB2* (refs. 5,6) and *GOSR2* (ref. 7) also contribute to cases of PME with preserved cognition. Other PMEs might have additional features, particularly dementia. PME-associated genes encode a variety of proteins, many of which are associated with endosomal and lysosomal function[8,9], but the associated disease mechanisms are generally poorly understood.

The precise clinical diagnosis of specific forms of PME is challenging because of genetic heterogeneity, phenotypic similarities and an overlap of symptoms with other epileptic and neurodegenerative diseases. In many cases, there are no distinguishing clinical features or biomarkers. Consequently, a substantial proportion of PME cases remain without a molecular diagnosis[3].

Here we aimed to identify the causative genes for unsolved PME cases by employing exome sequencing in unrelated individuals assembled from multiple centers in Europe, North America, Asia and Australia over a 25-year period. The extent of previous molecular studies varied, but all cases were negative for mutations in the *CSTB* gene and approximately half were negative for *SCARB2* and *GOSR2* mutations. The cohort was thus enriched for finding mutations in new genes and potential atypical phenotypes associated with known disease-related genes.

RESULTS

We performed exome sequencing on 84 unrelated PME cases, of which 70 were sporadic and 14 were from families with pedigrees suggestive of either dominant or recessive inheritance. We therefore analyzed the data seeking pathogenic autosomal recessive or dominant/*de novo*, sex-linked and mitochondrial DNA (mtDNA) variants (**Fig. 1** and Online Methods). On average, 4.15 Gb of sequence was produced within the exome bait regions, with an average coverage of 81 reads

A full list of affiliations appears at the end of the paper.

Received 8 July; accepted 16 October; published online 17 November 2014; doi:10.1038/ng.3144

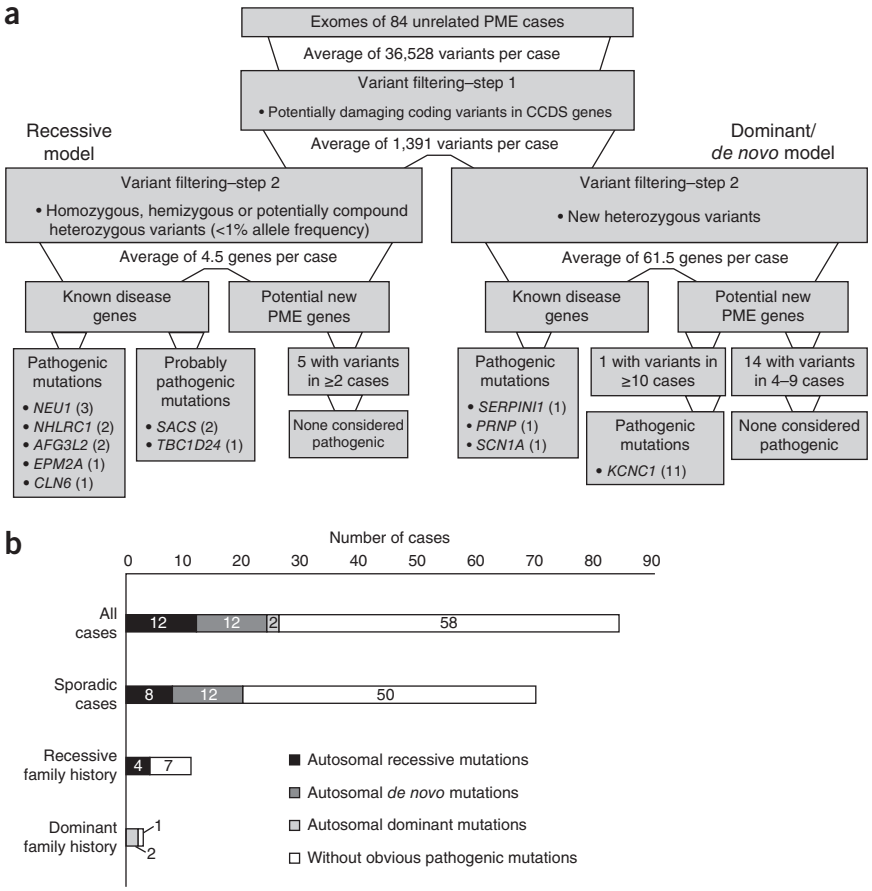

Figure 1 Analysis of the PME exomes. (**a**) A simplified flow chart of the exome data analysis strategy under autosomal or sex-linked recessive and dominant/*de novo* inheritance models and a summary of the results. The average total number of variants per exome (36,528) refers to single-nucleotide variants (SNVs) and indels passing quality filters within the exome bait regions. Numbers in parentheses after gene names indicate the number of cases with mutations in the gene. Gene and case counts under "potential new PME genes" are derived after excluding individuals with pathogenic or probably pathogenic mutations in known disease-related genes or with the pathogenic mutation in *KCNC1* identified in this study. (**b**) Numbers and proportions of cases without obvious pathogenic mutations or with pathogenic or probably pathogenic mutations of variable patterns of inheritance. The three cases with probably pathogenic mutations are included under sporadic cases with recessive mutations. Case PME84-1 with the recurrent *de novo* *KCNC1* mutation is included under cases with autosomal dominant mutations with a family history showing dominant inheritance (**Fig. 2a**).

per nucleotide (**Supplementary Table 1**). After filtering the raw variant data for possible pathogenic variants, we first analyzed the data for mutations in genes known to be associated with PME, epilepsy or neurodegenerative diseases and then performed analysis for new disease-related genes under both the recessive and dominant/*de novo* models. Analysis of the filtered variant data under the recessive model (**Fig. 1a**,**b**) identified pathogenic or probably pathogenic mutations (see the Online Methods for classification criteria) in known disease-causing genes in 12 cases. Analysis under the dominant/*de novo* model (**Fig. 1a**,**b**) led to the discovery of a new PME-associated gene, *KCNC1*, with, remarkably, the same recurrent *de novo* mutation in 11 cases and, in addition, identified pathogenic mutations in known disease-related genes in 3 cases. We did not identify any obvious pathogenic mutations in mtDNA. In total, we identified pathogenic or probably pathogenic mutations in 26 of 84 cases (31.0%).

Identification of a recurrent mutation in *KCNC1*

To identify new pathogenic mutations under the dominant/*de novo* model, we analyzed the data for potentially deleterious heterozygous variants that were absent in three variant databases. In addition, we did not consider variants in dbSNP except for those with a clinical association in the ClinVar database.

The highest number of new heterozygous variants occurred in *KCNC1* together with *TTN* (**Supplementary Table 2**). *TTN* encodes a large muscle protein and has a high mutational load[10] owing to its large coding region, and this gene was thus not considered further. We identified 11 (13.1%) unrelated cases with a new heterozygous c.959G>A mutation in *KCNC1* (**Supplementary Fig. 1**; Ensembl, ENST00000265969.6), which encodes potassium voltage-gated channel (K_V) subfamily C member 1 (KCNC1, also known as K_V3.1). The c.959G>A mutation causes a substitution of histidine for arginine at codon 320 of the K_V3.1 protein (p.Arg320His).

In all 11 cases, the mutation was confirmed by Sanger sequencing. The parents of all the cases positive for the c.959G>A mutation were unaffected, and segregation analysis for eight cases where both parental DNA samples were available showed that in each case the mutation occurred *de novo* (**Fig. 2a** and **Supplementary Fig. 2**). Genotyping a set of microsatellite markers in five trios with sufficient DNA available confirmed that the pedigrees were correct. One of the index cases (PME84-1) with the c.959G>A mutation had an affected sibling and two affected children, who were also each heterozygous for the mutation (**Fig. 2a**). The parents of PME84-1 and her unaffected brother were both negative for the mutation. The presence of two mutation-positive and clinically affected children from mutation-negative, unaffected parents suggests the occurrence of mosaicism in one of the parents. A restriction fragment length assay designed to detect both the normal and mutant alleles was carried out on peripheral blood DNA from both parents but showed no indication of mosaicism (data not shown).

We screened for the *KCNC1* c.959G>A mutation in a secondary cohort of 28 PME cases and identified 2 (7.1%) additional unrelated cases heterozygous for the mutation. Sanger sequencing of the available parental samples of one of these individuals confirmed the *de novo* occurrence of the mutation (**Fig. 2a**). In total, we identified 16 cases (13 unrelated) with the c.959G>A mutation. We did not identify any other mutations in *KCNC1* in the exome data. As exon 1 was not sufficiently covered, we carried out Sanger sequencing of it in the 73 exome-sequenced c.959G>A-negative cases, but no potentially deleterious variants were found.

The c.959G>A mutation in *KCNC1* affects a highly evolutionarily conserved arginine residue in segment S4, constituting the main voltage-sensing domain of the channel (**Fig. 2b**,**c**). The mutation was predicted to be deleterious by all four *in silico* methods used (**Supplementary Table 3**).

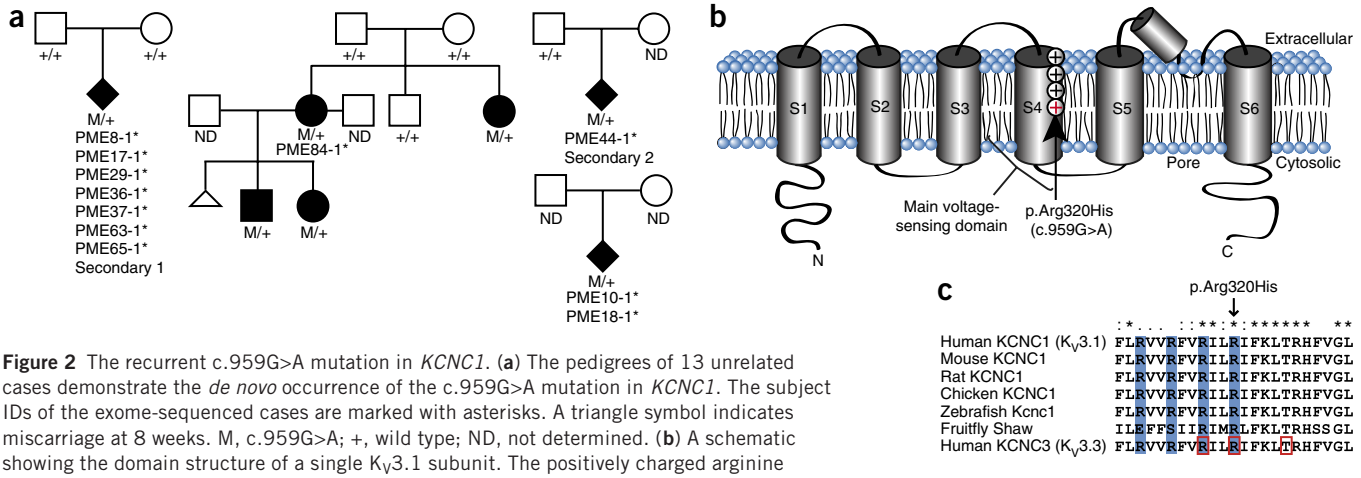

Figure 2 The recurrent c.959G>A mutation in *KCNC1*. (**a**) The pedigrees of 13 unrelated cases demonstrate the *de novo* occurrence of the c.959G>A mutation in *KCNC1*. The subject IDs of the exome-sequenced cases are marked with asterisks. A triangle symbol indicates miscarriage at 8 weeks. M, c.959G>A; +, wild type; ND, not determined. (**b**) A schematic showing the domain structure of a single $K_V3.1$ subunit. The positively charged arginine residues (marked with a plus sign) in the S4 segment detect changes in voltage. The p.Arg320His substitution changes one of the arginine residues to a histidine (red plus sign and arrow). (**c**) The ClustalX comparison of amino acid sequences for the voltage-sensing S4 segment shows full conservation of Arg320 (arrow) across different species. The four positively charged arginine residues (Arg311, Arg314, Arg317, Arg320) occurring every third position are highlighted in blue. The $K_V3.3$ residues Arg420, Arg423 and Thr428, mutated in spinocerebellar ataxia[24,25,27], are in red boxes. Asterisks, colons and periods indicate fully conserved, strongly similar and weakly similar residues, respectively.

To assess the frequency of PME due to *KCNC1* c.959G>A mutation, we used a newly published mutational model[10], which takes into account both the local sequence context of a mutation site and regional factors such as divergence between humans and macaques, to estimate the rate of this specific mutation. A rate of 1.75×10^{-7} mutations per person was obtained, indicating that the mutation should occur in 1 out of every 5,700,000 conceptions. Additionally, we examined three other potential mutations encoding changes of the conserved voltage-sensing arginine residues to histidine in segment S4 of $K_V3.1$ (p.Arg311His, p.Arg314His and p.Arg317His). Given that the sequence context of the four potential mutations is the same (they all occur in highly mutable CGC codons), the same estimated rate applied to all of them. If all 4 caused PME with equal penetrance, the probability of seeing only 1 of the 4 possible mutations in 13 of 13 independent cases is $P = 4 \times (1/4)^{13} = 6.0 \times 10^{-8}$, strongly suggesting that the effect of p.Arg320His is surprisingly specific for PME.

Functional analysis of p.Arg320His in the $K_V3.1$ channel

To assess the effects of the p.Arg320His substitution on channel function, we used the *Xenopus laevis* oocyte expression system and

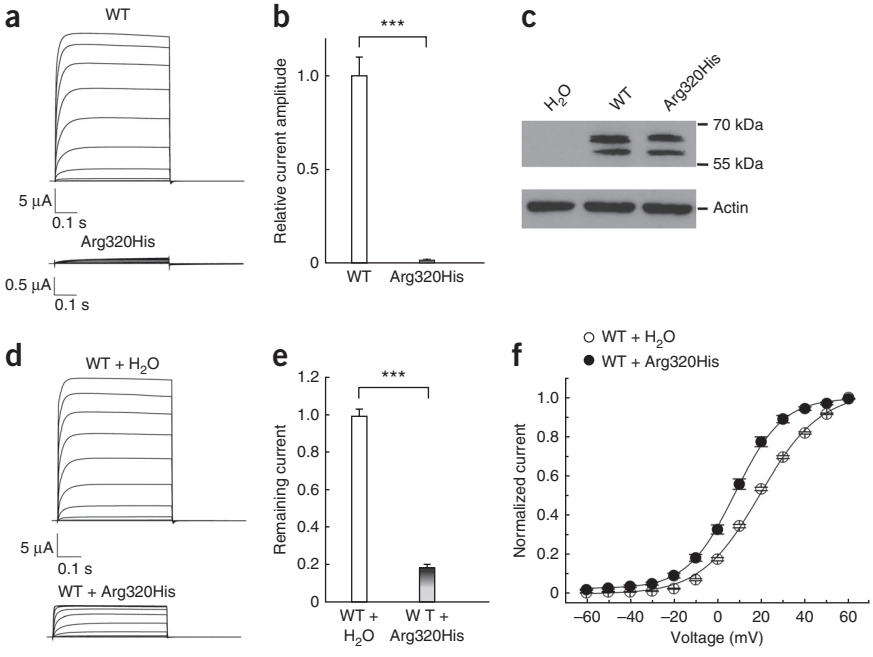

Figure 3 Functional analysis of the p.Arg320His substitution in $K_V3.1$. (**a**) Representative traces of whole-cell currents recorded in *X. laevis* oocytes, injected with the same amount of cRNA encoding wild-type (WT) or Arg320His $K_V3.1$, during 0.5-s voltage steps (–60 mV to +60 mV). (**b**) Relative current amplitudes of the wild-type channel ($n = 49$) and Arg320His mutant ($n = 50$) analyzed at the end of the voltage step to +60 mV and normalized to the mean current amplitude of the wild-type channel recorded on the same day (Mann-Whitney *U* test, $^{***}P < 0.001$). (**c**) Protein blot analysis of *X. laevis* oocytes injected with cRNA for either the wild-type channel or the Arg320His mutant using a mouse antibody to the DDK tag. Water-injected oocytes were used as a negative control, and actin served as a loading control. The presence of two bands on the blot is likely to be due to N-glycosylation of the $K_V3.1$ protein (expected protein size of ~56 kDa), which occurs in *in vivo* and in heterologous expression systems[50,51]. (**d**) Representative whole-cell currents from oocytes injected with a constant amount of cRNA for wild-type channel and either water or cRNA encoding Arg320His mutant in a 1:1 ratio, recorded as in **a**. (**e**) Relative current amplitudes remaining upon addition of Arg320His mutant to the wild-type channel ($n = 27$) were determined at the end of a 0.5-s pulse to +60 mV and normalized to the mean current amplitude for the wild-type channel coinjected with water ($n = 32$) recorded on the same day (Student's *t* test, $^{***}P < 0.001$). (**f**) The current-voltage relationships of cells expressing wild-type channel alone or the wild-type and Arg320His channels (Student's *t* test, $P < 0.001$ for –60 mV to +50 mV). Lines represent fits of a Boltzmann function. The potential of half-maximal activation ($V_{0.5}$) was 19.6 ± 0.5 mV ($n = 19$) and 8.0 ± 1.3 mV ($n = 16$) (Student's *t* test, $P < 0.001$) and the slope factor *k* was 12.9 ± 0.2 and 10.2 ± 0.3 (Student's *t* test, $P < 0.001$) for wild-type channel alone and the wild-type and Arg320His channels together, respectively. The data in **b**,**e** and **f** are presented as means ± s.e.m.

Table 1 Clinical features of cases with the c.959G>A mutation (p.Arg320His) in *KCNC1*

Case ID	Ancestry	Sex	Onset age (years)	Initial symptom	Seizures		Learning disability	Cognitive decline	Age (years); outcome
					Myoclonus	Tonic-clonic			
Exome-sequenced cases									
PME8-1	Italian	M	12	Myoclonus	+++	+	No	Yes	38; wheelchair at 27 years
PME10-1	Italian	M	6	Myoclonus	+++	++	No	Possible	34; wheelchair at 17 years
PME17-1	French	M	<5	Ataxia	+++	++	No	No	40; wheelchair at 16 years
PME18-1	Norwegian	F	10[a]	Myoclonus	+++	+	No	Yes	36; wheelchair at 15 years
PME29-1	German	M	9	Tremor/myoclonus	++	+	Yes	No	24; cautiously ambulant
PME36-1	US (Italian)	F	7	Tremor	+++	+	No	No	22; wheelchair at 14 years
PME37-1	Italian	F	10	Myoclonus	+++	+	No	No	19; wheelchair at 17 years
PME44-1	French Canadian	F	12	Myoclonus	++	+	No	Yes	24; walker at 17 years
PME63-1	Moldavian[b]	F	9	Myoclonus	+++	++	No	Possible[c]	15; wheelchair at 13 years
PME65-1	Portuguese	F	9	Myoclonus	+++	+	No	Yes	25; wheelchair at 19 years
PME84-1	Israeli (Sephardic)	F	10	Tremor	+	+	Yes	No	42; ambulant
Sanger-sequenced cases									
PME84-sister	Israeli (Sephardic)	F	13	Myoclonus	++	++	Yes	Yes	37; cautiously ambulant
PME84-son	Israeli (Sephardic)	M	12	Ataxia	+	+	Yes	Yes	19; cautiously ambulant
PME84-daughter	Israeli (Sephardic)	F	14	Tonic-clonic seizure	–	+	Yes	No	16; ambulant
Secondary 1	Danish	M	10[d]	Myoclonus	++	+	No	Yes	18; cautiously ambulant
Secondary 2	Israeli	M	NA	NA	NA	NA	NA	NA	NA

+, mild; ++, moderate; +++, severe; –, not observed. NA, data not available.
[a]Earlier absence seizures. [b]Ascertained in Italy. [c]Severe myoclonus and language barrier prevented good assessment. [d]Simple febrile seizures at 6–12 months.

automated two-electrode voltage clamp. Potassium currents were recorded from oocytes injected with identical amounts of wild-type or mutant cRNA for the human $K_V3.1$ channel. Whereas the wild-type channel produced robust currents upon membrane depolarization, the currents observed with the mutant channel were barely detectable (**Fig. 3a,b**). Immunoblot analysis using an antibody to the DDK tag with which both proteins were fused showed similar protein levels in the total lysates of oocytes expressing the wild-type or mutant subunit, indicating that the mutant protein had similar stability to the wild-type protein (**Fig. 3c**). To look for a possible interaction of the mutant subunit with the wild-type protein, we coexpressed the proteins at a 1:1 ratio. In these experiments, there was an approximately 80% reduction in the expected current amplitude recorded at +60 mV, indicating a dominant-negative effect of the mutant channel (**Fig. 3d,e**). The diminished currents resulting from the combination of the mutant and wild-type subunits demonstrated altered gating properties, with a significant hyperpolarizing shift of the activation curve ($P < 0.001$; **Fig. 3f**).

The clinical phenotype of cases with the *KCNC1* mutation

We obtained detailed clinical data for 15 of the 16 individuals positive for the *KCNC1* mutation (**Table 1**). The clinical phenotypes were similar and, at disease onset, resembled classic ULD. On a background of usually normal development, the first symptom in the majority of individuals was myoclonus (sometimes reported as tremor) at ages of 6–14 years. Ataxia developed early in one case (PME17-1), but it was otherwise overshadowed by myoclonus as the major motor impediment. There were infrequent tonic-clonic seizures in all cases. During adolescence, myoclonus generally became very severe, limiting ambulation; a walking aid or wheelchair was needed by mid to late teens. Learning disability before seizure onset was noted in some cases, in particular, the nuclear family of PME84-1. There was mild cognitive decline in seven subjects in early adolescence, but this was difficult to quantify owing to the severe motor disability. Early death was not observed. Electroencephalogram recordings showed generalized epileptiform discharges, with photosensitivity in some cases. Magnetic resonance imaging (MRI) scans had no specific features and were regarded as normal or showed cerebellar atrophy. The clinical picture in the family with four affected members (PME84) was milder, with the two older sisters ambulant in the fourth decade of life. Similarly, case 1 from the secondary cohort had a less severe clinical course than the majority of cases.

Mutations in known disease genes

Analysis for mutations in genes known to be associated with PME, epilepsy and neurodegenerative disease identified either pathogenic or probably pathogenic mutations in 15 of the 84 exome-sequenced cases (**Table 2**; see **Supplementary Table 4** for clinical details as well as summaries of the genetic findings, **Supplementary Fig. 3** for pedigrees with segregation data and **Supplementary Figs. 4** and **5** for conservation of the newly identified mutation sites). These genes fell into three groups.

First, ten cases had a recessively inherited or *de novo* heterozygous mutation in established PME-related genes, seven with atypical clinical presentations. The ten comprised three cases of Lafora disease (*NHLRC1* (ENST00000340650.3) and *EPM2A* (ENST00000367519.3)), three cases of sialidosis (*NEU1*; ENST00000375631.4) and one case of neuronal ceroid lipofuscinosis (*CLN6*; ENST00000249806.5). Two Italian cases, not known to be related, had the same new homozygous missense *AFG3L2* mutation (c.1875G>A; p.Met625Ile; ENST00000269143.3) affecting the proteolytic domain of the protein (**Supplementary Fig. 4e**). Exome data showed that they shared a ~1.75-Mb run of identical homozygous polymorphisms flanking the mutation, indicating that the mutation was identical by descent. The tenth case had a *de novo* previously described[11] pathogenic heterozygous missense mutation (c.1175G>A; p.Gly392Glu; ENST00000295777.5) in the *SERPINI1* gene encoding neuroserpin. Mutations in both *AFG3L2* and *SERPINI1* are very rare known causes of PME.

Second, four cases had mutations in known genes where PME has not been reported as a key part of clinical presentation. One case with adult-onset PME and a father who had died of a similar disease was found to have a previously described[12] pathogenic heterozygous missense mutation (c.305C>T; p.Pro102Leu; ENST00000379440.4) in the *PRNP* gene encoding prion protein. The mutation is a

known cause of Gerstmann-Sträussler-Scheinker disease, one of the inherited prion diseases. Two unrelated cases had probably pathogenic, rare compound heterozygous missense mutations in the *SACS* gene (c.8393C>A, p.Pro2798Gln in both cases; c.1373C>T, p.Thr458Ile and c.2996T>C, p.Ile999Thr in one case each; ENST00000382298.3). Two of the substitutions (p.Thr458Ile and p.Pro2798Gln) have been reported in individuals with spastic ataxia[13–15]. One case had a new probably pathogenic homozygous missense mutation (c.1079G>T; p.Arg360Leu; ENST00000293970.5) in *TBC1D24*, where recessive mutations cause variable neurological disorders, including familial infantile myoclonic epilepsy[16–20].

Third, in one case, we identified a previously seen[21] pathogenic heterozygous mutation (c.677C>T; p.Thr226Met; ENST00000303395.4) in *SCN1A*, the major gene underlying severe myoclonic epilepsy of infancy (Dravet syndrome)[22]. The eventual clinical evolution of this case was typical of Dravet syndrome and not PME. Initial consideration of PME as a clinical diagnosis was due to the predominance of myoclonic seizures in the early disease course.

All variants passing filtering in the known disease-related genes, including the ones not considered to be pathogenic or probably pathogenic, are listed in **Supplementary Tables 5** (recessive) and **6** (dominant/*de novo*).

Table 2 Pathogenic or probably pathogenic mutations in known PME, epilepsy or neurodegenerative disease genes

Case ID, sex	Gene	Zygosity	Coding DNA change[a]	Protein change[a]	CADD, SIFT, PolyPhen, MutationTaster predictions[b]	Allele frequency in 1000G/ EVS (%)[c]	Previously reported pathogenic mutation (reference)	Disease associated with the gene (OMIM gene number)
Pathogenic recessive mutations								
PME23-1, F	*NEU1*	Het	c.1208delG	p.Ser403Thrfs*85	32, NA, NA, NA	0/0	Yes (ref. 52)	PME; sialidosis (608272)
		Het	c.982G>A	p.Gly328Ser	32, D, D, D	0/0	Yes (ref. 53)	
PME51-1, F	*NEU1*	Het	c.982G>A	p.Gly328Ser	32, D, D, D	0/0	Yes (ref. 53)	
		Het	c.679G>A	p.Gly227Arg	28.5, D, D, D	0/0	Yes (ref. 53)	
PME87-1, F	*NEU1*	Het	c.914G>A	p.Arg305His	9.4, B, PD, D	0/0	No, but p.Arg305Cys is reported (ref. 54)	
		Het	c.625delG	p.Glu209Serfs*94	26.1, NA, NA, NA	0/0	Yes (ref. 53)	
PME35-1, F	*NHLRC1*	Hom	c.436G>A	p.Asp146Asn	15.75, B, PD, D	0/0	Yes (ref. 55)	PME; Lafora disease (608072)
PME81-1, M	*NHLRC1*	Hom	c.830C>A	p.Ala277Glu	12.72, D, D, D	0/0	No	
PME82-1, M	*EPM2A*	Hom	c.590A>T	p.Asp197Val	27.4, D, D, D	0/0	No	PME; Lafora disease (607566)
PME33-1, M	*CLN6*	Hom	c.509A>G	p.Tyr170Cys	17.11, D, D, D	0/0	No	PME: neuronal ceroid lipofuscinosis (606725)
PME62-1, M	*AFG3L2*	Hom	c.1875G>A	p.Met625Ile	30, B, PD, D	0/0	No	Spinocerebellar ataxia 28 and spastic ataxia with PME (604581)
PME32-1, F	*AFG3L2*	Hom	c.1875G>A	p.Met625Ile	30, B, PD, D	0/0	No	
Probably pathogenic recessive mutations								
PME14-1, F	*TBC1D24*	Hom	c.1079G>T	p.Arg360Leu	19.83, D, D, D	0/0	No	Multiple neurological diseases (613577); PME not previously described
PME15-1, F	*SACS*	Het	c.8393C>A	p.Pro2798Gln	25.7, D, D, D	0.09/0.29	Possible (ref. 13)[d]	Autosomal recessive spastic ataxia of the Charlevoix Saguenay (604490); PME not previously described
		Het	c.2996T>C	p.Ile999Thr	17.35, D, B, D	0/0.015	No	
PME75-1, F	*SACS*	Het	c.8393C>A	p.Pro2798Gln	25.7, D, D, D	0.09/0.29	Possible (ref. 13)[d]	
		Het	c.1373C>T	p.Thr458Ile	17.45, D, D, D	0.14/0.24	Possible (ref. 15)[d] and yes (ref. 14)	
Pathogenic dominant/*de novo* mutations								
PME42-1, F	*SERPINI1*	Het	c.1175G>A	p.Gly392Glu	22.5, D, D, D	0/0	Yes (ref. 11)	PME; familial encephalopathy with neuroserpin inclusion bodies (604218)
PME86-1, F	*PRNP*	Het	c.305C>T	p.Pro102Leu	19.12, D, D, D	0/0	Yes (ref. 12)	Gerstmann-Sträussler-Scheinker disease (176640); PME not previously described
PME20-1, F	*SCN1A*	Het	c.677C>T	p.Thr226Met	20.5, D, D, D	0/0	Yes (ref. 21)	Dravet syndrome (182389)

Hom, homozygous; het, heterozygous; M, male; F, female.
[a]Genomic positions and more detailed annotations of the mutations are presented in **Supplementary Table 3**. Mutation coding DNA and amino acid positions are based on Ensembl transcripts (see main text). [b]A CADD score of >15 indicates deleteriousness for the variant (Online Methods). B, benign (not considered deleterious by the method); PD, possibly deleterious (applies to PolyPhen only); D, deleterious; NA, not available. [c]1000G, 1000 Genomes Project; EVS, Exome Variant Server of the National Heart, Lung, and Blood Institute (NHLBI) Exome Sequencing Project. [d]See the **Supplementary Note** for a discussion of the pathogenicity of the previously reported *SACS* mutations.

Search for additional genes with new mutations

We analyzed the exome data set for potential new PME-associated genes aside from *KCNC1*, using both recessive and dominant/*de novo* models. We did not identify other likely new genes using our criteria of observing putative mutations in a gene in at least two unsolved cases under the recessive model or in at least four unsolved cases using the dominant/*de novo* model (**Supplementary Tables 2** and **7**, and **Supplementary Note**). However, genes of interest in single cases that would warrant further exploration include *ALG10* and *APOA1BP*, which harbored homozygous loss-of-function mutations (**Supplementary Table 8**).

DISCUSSION

Using an exome sequencing approach in a clinically heterogeneous cohort of 84 unrelated individuals with PME without a specific cause, we reached a genetic diagnosis in 31% of the cases. Notably, we identified a recurrent mutation in *KCNC1* as a new cause of PME that explained a substantial proportion of cases. *KCNC1* encodes $K_V3.1$, which functions as a highly conserved[23] potassium ion channel subunit of the K_V3 subfamily of voltage-gated tetrameric potassium ion channels. Although *KCNC1* mutations have not been associated with human disease until now, mutations inherited in an autosomal dominant manner or occurring *de novo* in *KCNC3* ($K_V3.3$) cause spinocerebellar ataxia[24–27].

K_V3 channel subunits consist of six membrane-spanning segments (S1–S6), have overlapping expression patterns and can form heterotetramers[28]. S4 constitutes the main voltage sensor where specific positively charged arginine residues contribute to the gating charge[29,30]. Electrophysiological analysis showed that the PME-causing p.Arg320His substitution, which affects one of the voltage-sensing residues, causes prominent loss of function with a dominant-negative effect on wild-type $K_V3.1$ channels. We also observed altered gating properties for the mutant protein, but the physiological consequence of this finding is questionable, as the overall contribution of these altered properties to $K_V3.1$-mediated current is minor. Similar biophysical properties have been reported for an ataxia-causing alteration in $K_V3.3$, p.Arg423His[31], occurring in the position analogous to p.Arg320His in $K_V3.1$. Mutations affecting positively charged residues in segment S4 of voltage-gated cation channels might contribute to pathogenicity by generating leak currents through the gating pore[32]. For example, in the *Drosophila Shaker* K_V channel, the change analogous to p.Arg320His in $K_V3.1$ increases proton permeability[33]. However, gating pore currents are not detectable for the analogous $K_V3.3$ mutant[31], calling into question the importance of the phenomenon in the context of $K_V3.1$. Given the ability of K_V3 subunits to form heterotetramers, the dominant-negative Arg320His $K_V3.1$ mutant is likely to disrupt all K_V3-mediated currents of the neurons in which it is expressed. Reflecting functional redundancy, *Kcnc1* and *Kcnc3* knockout mice have relatively mild phenotypes, whereas double-mutant mice show myoclonus, tremor and gait ataxia[34–36]. Thus, the dominant-negative $K_V3.1$ and $K_V3.3$ mutations identified in cases seem to have an effect comparable to double knockout in mice.

The K_V3 subfamily is distinguished from other K_V channels by more positively shifted voltage-dependent activation and faster activation and deactivation rates. These differences make K_V3 channels major determinants of high-frequency firing in several types of central nervous system (CNS) neurons[28]. Studies using mutant or pharmacologically suppressed K_V3 channels have demonstrated that loss of K_V3 function disrupts the firing properties of fast-spiking neurons[28,37,38], affects neurotransmitter release[39] and induces cell death[40]. The expression of $K_V3.1$ is limited to the CNS, with the exception of a subpopulation of T lymphocytes[41,42]. It is preferentially expressed in specific subsets of fast-spiking neurons, with prominent expression in inhibitory GABAergic interneurons[28,41]. Therefore, it is likely that the p.Arg320His substitution in $K_V3.1$ results in disinhibition due to the impaired firing of fast-spiking GABAergic interneurons. This mechanism is likely to contribute particularly to myoclonus and tonic-clonic seizures. Furthermore, dysfunction and/or degeneration of cerebellar neurons, where $K_V3.1$ is expressed[41], are likely to contribute to motor impairment. Modulation of K_V3 channel function may provide a possibility for pharmacological intervention in patients with *KCNC1* mutations. However, although drugs with anticonvulsant effects activating other K_V channels exist[43], there is no activator of K_V3 channels currently available.

The initial clinical presentation and evolution of ULD[44] and the disorder in individuals with the *KCNC1* mutation, designated here as 'MEAK' (myoclonus epilepsy and ataxia due to potassium channel mutation), are similar. They have overlapping ages of onset and moderate-to-severe incapacitating myoclonus, infrequent tonic-clonic seizures and mild, if any, cognitive decline. Differences emerge later in disease progression, as the clinical course for MEAK is generally more severe. ULD is caused by mutations in *CSTB*, encoding cystatin B, which is implicated in oxidative stress and inflammation[45,46]. Evidence from the mouse model for ULD suggests that altered GABAergic signaling contributes to latent hyperexcitability[47,48], implying a possible convergent pathway for ULD and MEAK.

The recurrence of the *KCNC1* mutation is likely due to its location in a CpG dinucleotide, corresponding to a class of sites that represent mutation hotspots[49]. We estimated that the mutation occurs in 1 out of 5,700,000 conceptions, thus potentially affecting hundreds of individuals globally. The observation of four cases positive for the *KCNC1* mutation ascertained in a multicenter clinical collaboration in Italy[3] supports this estimate, assuming that probably not all existing cases were ascertained and that the mutation might reduce lifespan. We did not observe any other mutations in *KCNC1*, which is among the top 1% of the most constrained genes[10]. For example, the estimated mutation rates for the three other potential arginine-to-histidine substitutions affecting voltage-sensing residues are equal to that for p.Arg320His, and these mutations thus should have been observed in our cohort if the phenotypic consequences were the same. The fact that we only identified the mutation affecting Arg320 suggests that this residue is biophysically special. Indeed, codon-specific consequences of S4-altering mutations have been demonstrated, for example, in $K_V3.3$ (ref. 31).

The identification of mutations in previously established disease-related genes expands the phenotypic and genotypic spectra of PME. Highlighting the usefulness of exome sequencing as a diagnostic tool in a heterogeneous cohort of affected individuals previously subjected to molecular analyses, we identified pathogenic mutations in known PME-associated genes in ten individuals, of whom the majority had atypical symptoms (**Supplementary Table 4** and **Supplementary Note**). Notably, we identified mutations in three known disease-related genes (*PRNP*, *SACS* and *TBC1D24*), where PME has not been appreciated as part of the clinical spectrum. These cases are discussed in the **Supplementary Note**. The majority of all solved cases also had variants in other known disease-associated genes (**Supplementary Tables 5** and **6**). These variants, however, did not fulfill our criteria for pathogenicity. It is possible that they modify the clinical outcome, thus contributing to some atypical disease presentations.

The genetic basis of disease remained unknown in over two-thirds of the cases. Aside from *KCNC1*, there were no other new PME-related

genes definitively identified (**Supplementary Tables 2** and **7**, and **Supplementary Note**); however, of the nine genes with homozygous loss-of-function mutations in single cases, some are interesting candidates (**Supplementary Table 8**). In light of *de novo* mutations being established as an important cause of PME, exome sequencing in a family trio setting could be pursued to further dissect this heterogeneous cohort. Also, the role of copy number variants (CNVs) and epistatic mutations in PMEs should be assessed. Our findings, especially the discovery of MEAK, will aid in molecular diagnostics and potential therapeutic interventions in PME, and the exome data generated will facilitate the further identification of disease-relevant genes.

URLs. CADD, http://cadd.gs.washington.edu/; Epilepsy and neurodegenerative disease gene panels (accessed February 2014), http://www.cegat.de/en/services/diagnostic-panels/; ClustalX, http://www.ebi.ac.uk/Tools/msa/clustalw2/; Exome Variant Server of the National Heart, Lung, and Blood Institute Grand Opportunity (NHLBI GO) Exome Sequencing Project (accessed February 2014), http://evs.gs.washington.edu/EVS/; Genome Analysis Toolkit (GATK), http://www.broadinstitute.org/gatk/; Genotype-Tissue Expression (GTEx) Project, http://www.gtexportal.org/; MITOMAP (accessed February 2014), http://www.mitomap.org/; NCBI ClinVar database, http://www.ncbi.nlm.nih.gov/clinvar/; Online Mendelian Inheritance in Man (OMIM) (accessed February 2014), http://omim.org/; Picard, http://broadinstitute.github.io/picard/; Primer-BLAST, http://www.ncbi.nlm.nih.gov/tools/primer-blast/; Sequencing Initiative Suomi (SISu), http://sisuproject.fi/; UCSC Genome Browser, http://genome.ucsc.edu/; UniProt database, http://www.uniprot.org/.

METHODS

Methods and any associated references are available in the online version of the paper.

Accession codes. Raw aligned sequence reads have been submitted to the European Genome-phenome Archive (EGA) by the Wellcome Trust Sanger Institute under study accessions EGAS00001000048 and EGAS00001000386.

Note: Any Supplementary Information and Source Data files are available in the online version of the paper.

ACKNOWLEDGMENTS

We thank the patients and family members who contributed samples for the purpose of this study. We also thank the following for patient referrals: K. Joost, K. Carvalho, C. Marques Lourenco, P. Cossette, A. Covanis, A. Parmeggiani, P. Van Bogaert, S. Mole, A. Sierra Marcos, M. Carreno and S.S. Rich. We thank P. Hakala, E. Hämäläinen, B. Johns, R. Schulz, J. Damiano, H. Löffler and N. Jezutkovic for sample logistics and technical assistance in the laboratory, C. Scott and J. Durham (Wellcome Trust Sanger Institute) for exome sequence processing, P. Gormley, B. Winsvold and P. Palta for assistance in exome data analysis, and A. Farooq Bazai for support. CSC–IT Center for Science, Ltd., is acknowledged for the allocation of computational resources.

This study was supported by the Folkhälsan Research Foundation (A.-E.L.), Academy of Finland grant 141549 (A.-E.L.), Wellcome Trust grants 089062 and 098051 (A.P.), European Commission Framework Programme 7 (FP7) project 201413 ENGAGE (A.P.), project 242167 SynSys (A.P.), Health-2010 projects 261433 BioSHare (A.P.) and project 261123 gEUVADIS (A.P.), Academy of Finland grants 251704 and 263401 (A.P.), the Sigrid Juselius Foundation (A.P.), US NIH grant RFA-HL-12-007 (A.P.), the Emil Aaltonen Foundation (M.M.), Epilepsiatutkimussäätiö (M.M.), University of Helsinki Funds (M.M.), the Doctoral Programme in Biomedicine (M.M.), National Health and Medical Research Council (NHMRC) of Australia program grant 628952 (S.F.B., L.M.D. and I.E.S.), NHMRC Career Development Fellowship 1032603 (L.M.D.), NHMRC Early Career Fellowship 1016715 (S.E.H.), the German Network for Rare Diseases of the Federal Ministry of Education and Research (BMBF), IonNeurONet 01GM1105A (S. Maljevic and H.L.), the EuroEPINOMICS program of the European Science Foundation, German Research Foundation (DFG) grant Le1030/11-1 (H.L. and S. Maljevic), NHMRC program grant 400121 (S.P.) and NMHRC fellowship 1005050 (S.P.). The Florey Institute of Neuroscience and Mental Health (S.P.) is supported by government infrastructure funds from the state of Victoria.

AUTHOR CONTRIBUTIONS

Study design and management: S.F.B., L.M.D., A.P. and A.-E.L. Coordination of the collection of study subjects and clinical data: S.F.B., K.L.O., M.A.B. and A.-E.L. Subject ascertainment and phenotyping: S.F.B., K.L.O., L.C., S.F., R.M., E.A., F.A., A.G., P.T., L.L., I.E.S., C.C., A.F., E.F., J.A., A.A., B.B., E.S., M.T., P.R., M.D.K., C.O., D.M.A., B.A.E., A.C., M.L., E.L., V.S., J.M., M.P., A.J.E., B.K., M.D., R.S.M., R.S., Z.A. and B.B.-Z. Analysis of the exome sequencing data: M.M. and S. Markkinen. Sanger sequencing, sequence data analysis and mosaicism analysis: M.M., M.A.B., T.J., S.E.H. and M.S.H. Interpretation of genetic data: M.M., S.F.B., L.M.D., A.P. and A.-E.L. Evaluation of the mutation rate in *KCNC1*: K.E.S. and M.J.D. Functional analysis and interpretation: S. Maljevic, S.P. and H.L. Manuscript writing: M.M., S.F.B., L.M.D., K.L.O., S. Maljevic, H.L., A.P. and A.-E.L. All authors critically revised the manuscript.

COMPETING FINANCIAL INTERESTS

The authors declare no competing financial interests.

1. Berkovic, S.F., Andermann, F., Carpenter, S. & Wolfe, L.S. Progressive myoclonus epilepsies: specific causes and diagnosis. *N. Engl. J. Med.* **315**, 296–305 (1986).
2. Shahwan, A., Farrell, M. & Delanty, N. Progressive myoclonic epilepsies: a review of genetic and therapeutic aspects. *Lancet Neurol.* **4**, 239–248 (2005).
3. Franceschetti, S. *et al.* Progressive myoclonic epilepsies: definitive and still undetermined causes. *Neurology* **82**, 405–411 (2014).
4. Pennacchio, L.A. *et al.* Mutations in the gene encoding cystatin B in progressive myoclonus epilepsy (EPM1). *Science* **271**, 1731–1734 (1996).
5. Berkovic, S.F. *et al.* Array-based gene discovery with three unrelated subjects shows SCARB2/LIMP-2 deficiency causes myoclonus epilepsy and glomerulosclerosis. *Am. J. Hum. Genet.* **82**, 673–684 (2008).
6. Dibbens, L.M. *et al. SCARB2* mutations in progressive myoclonus epilepsy (PME) without renal failure. *Ann. Neurol.* **66**, 532–536 (2009).
7. Corbett, M.A. *et al.* A mutation in the Golgi Qb-SNARE gene *GOSR2* causes progressive myoclonus epilepsy with early ataxia. *Am. J. Hum. Genet.* **88**, 657–663 (2011).
8. Kollmann, K. *et al.* Cell biology and function of neuronal ceroid lipofuscinosis–related proteins. *Biochim. Biophys. Acta* **1832**, 1866–1881 (2013).
9. Ramachandran, N., Girard, J.-M., Turnbull, J. & Minassian, B.A. The autosomal recessively inherited progressive myoclonus epilepsies and their genes. *Epilepsia* **50**, 29–36 (2009).
10. Samocha, K.E. *et al.* A framework for the interpretation of *de novo* mutation in human disease. *Nat. Genet.* **46**, 944–950 (2014).
11. Davis, R.L. *et al.* Association between conformational mutations in neuroserpin and onset and severity of dementia. *Lancet* **359**, 2242–2247 (2002).
12. Hsiao, K. *et al.* Linkage of a prion protein missense variant to Gerstmann-Straussler syndrome. *Nature* **338**, 342–345 (1989).
13. Baets, J. *et al.* Mutations in *SACS* cause atypical and late-onset forms of ARSACS. *Neurology* **75**, 1181–1188 (2010).
14. Romano, A. *et al.* Comparative analysis and functional mapping of *SACS* mutations reveal novel insights into sacsin repeated architecture. *Hum. Mutat.* **34**, 525–537 (2013).
15. Synofzik, M. *et al.* Autosomal recessive spastic ataxia of Charlevoix Saguenay (ARSACS): expanding the genetic, clinical and imaging spectrum. *Orphanet J. Rare Dis.* **8**, 41 (2013).
16. Afawi, Z. *et al. TBC1D24* mutation associated with focal epilepsy, cognitive impairment and a distinctive cerebro-cerebellar malformation. *Epilepsy Res.* **105**, 240–244 (2013).
17. Campeau, P.M. *et al.* The genetic basis of DOORS syndrome: an exome-sequencing study. *Lancet Neurol.* **13**, 44–58 (2014).
18. Corbett, M.A. *et al.* A focal epilepsy and intellectual disability syndrome is due to a mutation in *TBC1D24*. *Am. J. Hum. Genet.* **87**, 371–375 (2010).
19. Falace, A. *et al.* TBC1D24, an ARF6-interacting protein, is mutated in familial infantile myoclonic epilepsy. *Am. J. Hum. Genet.* **87**, 365–370 (2010).
20. Guven, A. & Tolun, A. *TBC1D24* truncating mutation resulting in severe neurodegeneration. *J. Med. Genet.* **50**, 199–202 (2013).
21. Harkin, L.A. *et al.* The spectrum of *SCN1A*-related infantile epileptic encephalopathies. *Brain* **130**, 843–852 (2007).
22. Claes, L. *et al. De novo* mutations in the sodium-channel gene *SCN1A* cause severe myoclonic epilepsy of infancy. *Am. J. Hum. Genet.* **68**, 1327–1332 (2001).

23. Ried, T. *et al.* Localization of a highly conserved human potassium channel gene (*NGK2-KV4*; *KCNC1*) to chromosome 11p15. *Genomics* **15**, 405–411 (1993).
24. Waters, M.F. *et al.* Mutations in voltage-gated potassium channel *KCNC3* cause degenerative and developmental central nervous system phenotypes. *Nat. Genet.* **38**, 447–451 (2006).
25. Figueroa, K.P. *et al.* KCNC3: phenotype, mutations, channel biophysics—a study of 260 familial ataxia patients. *Hum. Mutat.* **31**, 191–196 (2010).
26. Figueroa, K.P. *et al.* Frequency of *KCNC3* DNA variants as causes of spinocerebellar ataxia 13 (SCA13). *PLoS ONE* **6**, e17811 (2011).
27. Németh, A.H. *et al.* Next generation sequencing for molecular diagnosis of neurological disorders using ataxias as a model. *Brain* **136**, 3106–3118 (2013).
28. Rudy, B. & McBain, C.J. Kv3 channels: voltage-gated K^+ channels designed for high-frequency repetitive firing. *Trends Neurosci.* **24**, 517–526 (2001).
29. Seoh, S.-A., Sigg, D., Papazian, D.M. & Bezanilla, F. Voltage-sensing residues in the S2 and S4 segments of the *Shaker* K^+ channel. *Neuron* **16**, 1159–1167 (1996).
30. Aggarwal, S.K. & MacKinnon, R. Contribution of the S4 segment to gating charge in the *Shaker* K^+ channel. *Neuron* **16**, 1169–1177 (1996).
31. Minassian, N.A., Lin, M.-C.A. & Papazian, D.M. Altered $K_V3.3$ channel gating in early-onset spinocerebellar ataxia type 13. *J. Physiol. (Lond.)* **590**, 1599–1614 (2012).
32. Moreau, A., Gosselin-Badaroudine, P. & Chahine, M. Biophysics, pathophysiology, and pharmacology of ion channel gating pores. *Front. Pharmacol.* **5**, 53 (2014).
33. Starace, D.M. & Bezanilla, F. Histidine scanning mutagenesis of basic residues of the S4 segment of the *Shaker* K^+ channel. *J. Gen. Physiol.* **117**, 469–490 (2001).
34. Ho, C.S., Grange, R.W. & Joho, R.H. Pleiotropic effects of a disrupted K^+ channel gene: reduced body weight, impaired motor skill and muscle contraction, but no seizures. *Proc. Natl. Acad. Sci. USA* **94**, 1533–1538 (1997).
35. Joho, R.H., Ho, C.S. & Marks, G.A. Increased γ- and decreased δ-oscillations in a mouse deficient for a potassium channel expressed in fast-spiking interneurons. *J. Neurophysiol.* **82**, 1855–1864 (1999).
36. Espinosa, F. *et al.* Alcohol hypersensitivity, increased locomotion, and spontaneous myoclonus in mice lacking the potassium channels $K_V3.1$ and $K_V3.3$. *J. Neurosci.* **21**, 6657–6665 (2001).
37. Issa, F.A., Mazzochi, C., Mock, A.F. & Papazian, D.M. Spinocerebellar ataxia type 13 mutant potassium channel alters neuronal excitability and causes locomotor deficits in zebrafish. *J. Neurosci.* **31**, 6831–6841 (2011).
38. Erisir, A., Lau, D., Rudy, B. & Leonard, C.S. Function of specific K^+ channels in sustained high-frequency firing of fast-spiking neocortical interneurons. *J. Neurophysiol.* **82**, 2476–2489 (1999).
39. Sabatini, B.L. & Regehr, W.G. Control of neurotransmitter release by presynaptic waveform at the granule cell to Purkinje cell synapse. *J. Neurosci.* **17**, 3425–3435 (1997).
40. Irie, T., Matsuzaki, Y., Sekino, Y. & Hirai, H. $K_V3.3$ channels harbouring a mutation of spinocerebellar ataxia type 13 alter excitability and induce cell death in cultured cerebellar Purkinje cells. *J. Physiol. (Lond.)* **592**, 229–247 (2014).
41. Gan, L. & Kaczmarek, L.K. When, where, and how much? Expression of the $K_V3.1$ potassium channel in high-frequency firing neurons. *J. Neurobiol.* **37**, 69–79 (1998).
42. GTEx Consortium. The Genotype-Tissue Expression (GTEx) project. *Nat. Genet.* **45**, 580–585 (2013).
43. Wulff, H., Castle, N.A. & Pardo, L.A. Voltage-gated potassium channels as therapeutic targets. *Nat. Rev. Drug Discov.* **8**, 982–1001 (2009).
44. Kälviäinen, R. *et al.* Clinical picture of EPM1-Unverricht-Lundborg disease. *Epilepsia* **49**, 549–556 (2008).
45. Lehtinen, M.K. *et al.* Cystatin B deficiency sensitizes neurons to oxidative stress in progressive myoclonus epilepsy, EPM1. *J. Neurosci.* **29**, 5910–5915 (2009).
46. Okuneva, O. *et al.* Abnormal microglial activation in the *Cstb*$^{-/-}$ mouse, a model for progressive myoclonus epilepsy, EPM1. *Glia.* doi:10.1002/glia.22760 (18 October 2014)
47. Buzzi, A. *et al.* Loss of cortical GABA terminals in Unverricht-Lundborg disease. *Neurobiol. Dis.* **47**, 216–224 (2012).
48. Joensuu, T. *et al.* Gene expression alterations in the cerebellum and granule neurons of *Cstb*$^{-/-}$ mouse are associated with early synaptic changes and inflammation. *PLoS ONE* **9**, e89321 (2014).
49. Kong, A. *et al.* Rate of *de novo* mutations and the importance of father's age to disease risk. *Nature* **488**, 471–475 (2012).
50. Brooks, N.L., Corey, M.J. & Schwalbe, R.A. Characterization of N-glycosylation consensus sequences in the $K_V3.1$ channel. *FEBS J.* **273**, 3287–3300 (2006).
51. Hall, M.K., Cartwright, T.A., Fleming, C.M. & Schwalbe, R.A. Importance of glycosylation on function of a potassium channel in neuroblastoma cells. *PLoS ONE* **6**, e19317 (2011).
52. Bonten, E., van der Spoel, A., Fornerod, M., Grosveld, G. & d'Azzo, A. Characterization of human lysosomal neuraminidase defines the molecular basis of the metabolic storage disorder sialidosis. *Genes Dev.* **10**, 3156–3169 (1996).
53. Lukong, K.E. *et al.* Characterization of the sialidase molecular defects in sialidosis patients suggests the structural organization of the lysosomal multienzyme complex. *Hum. Mol. Genet.* **9**, 1075–1085 (2000).
54. Canafoglia, L. *et al.* Expanding sialidosis spectrum by genome-wide screening: *NEU1* mutations in adult-onset myoclonus. *Neurology* **82**, 2003–2006 (2014).
55. Chan, E.M. *et al.* Mutations in *NHLRC1* cause progressive myoclonus epilepsy. *Nat. Genet.* **35**, 125–127 (2003).

[1]Institute for Molecular Medicine Finland, University of Helsinki, Helsinki, Finland. [2]Folkhälsan Institute of Genetics, Helsinki, Finland. [3]Neuroscience Center, University of Helsinki, Helsinki, Finland. [4]Research Programs Unit, Molecular Neurology, University of Helsinki, Helsinki, Finland. [5]Epilepsy Research Center, Department of Medicine, University of Melbourne, Austin Health, Heidelberg, Victoria, Australia. [6]School of Pharmacy and Medical Sciences, University of South Australia, Adelaide, South Australia, Australia. [7]Department of Neurology and Epileptology, Hertie Institute for Clinical Brain Research, University of Tübingen, Tübingen, Germany. [8]Department of Neurophysiopathology, C. Besta Foundation Neurological Institute, Istituto di Ricerca e Cura a Carattere Scientifico (IRCCS), Milan, Italy. [9]Neurology Unit, IRCCS Institute of Neurological Sciences of Bologna, Bellaria Hospital, Bologna, Italy. [10]Montreal Neurological Institute, McGill University, Montreal, Quebec, Canada. [11]Institute of Neurology, University Magna Graecia, Catanzaro, Italy. [12]Department of Biomedical and Neuromotor Sciences, University of Bologna, Bologna, Italy. [13]Florey Institute of Neuroscience and Mental Health, University of Melbourne, Melbourne, Victoria, Australia. [14]Department of Pediatrics, Royal Children's Hospital, University of Melbourne, Melbourne, Victoria, Australia. [15]Department of Neurosciences, Reproductive Sciences and Odontostomatology, Federico II University, Naples, Italy. [16]Department of Medical and Surgical Sciences, Magna Graecia University, Catanzaro, Italy. [17]Regional Epilepsy Center, Bianchi-Melacrino-Morelli Hospital, Reggio Calabria, Italy. [18]Department of Biotechnology and Informatics, Balochistan University of Information Technology, Engineering and Management Sciences, Quetta, Pakistan. [19]Department of Medicine, Mayo Hospital, Lahore, Pakistan. [20]Department of Neurology, Istanbul Faculty of Medicine, Istanbul University, Istanbul, Turkey. [21]Epilepsy Center (EPIMER), Istanbul University, Istanbul, Turkey. [22]Department of Anatomy and Cell Biology, University of Malta, Msida, Malta. [23]Section of Medical Genetics, Mater dei Hospital, Msida, Malta. [24]Division of Pediatric Neurology, Department of Pediatrics, Hacettepe University Faculty of Medicine, Ankara, Turkey. [25]Department of Neurology, Temple Street Children's University Hospital, Dublin, Ireland. [26]Academic Centre on Rare Diseases, School of Medicine and Medical Science, University College Dublin, Dublin, Ireland. [27]Department of Neurology, Cerrahpasa Medical Faculty, Istanbul University, Istanbul, Turkey. [28]Division of Neurology, Department of Medicine, University of Toronto, Toronto Western Hospital, Krembil Neurosciences Program, Toronto, Ontario, Canada. [29]Department of Clinical Medicine, University of Bergen, Bergen, Norway. [30]Department of Neurology, Haukeland University Hospital, Bergen, Norway. [31]Epilepsy Unit, Hôpital Gui de Chauliac, Montpellier, France. [32]Department of Neurology and Epileptology, Epilepsy Center Hamburg-Alsterdorf, Hamburg, Germany. [33]Department of Neurodegenerative Diseases, Hertie Institute for Clinical Brain Research, University of Tübingen, Tübingen, Germany. [34]German Center for Neurodegenerative Diseases (DZNE), Tübingen, Germany. [35]Developmental Neurology Unit, C. Besta Foundation Neurological Institute, IRCCS, Milan, Italy. [36]Department of Neurology, Centro Hospitalar São João, Porto, Portugal. [37]Department of Clinical Neurosciences and Mental Health, Faculty of Medicine, University of Porto, Porto, Portugal. [38]Epilepsy Center, University of Cincinnati Neuroscience Institute, Cincinnati, Ohio, USA. [39]Gardner Center for Parkinson Disease and Movement Disorders, University of Cincinnati, Cincinnati, Ohio, USA. [40]Klinikum Links der Weser, Bremen, Germany. [41]Brain Institute, Miami Children's Hospital, Miami, Florida, USA. [42]Department of Neurology, University of Miami Miller School of Medicine, Miami, Florida, USA. [43]Danish Epilepsy Centre, Dianalund, Denmark. [44]Institute of Regional Health Services Research, University of Southern Denmark, Odense, Denmark. [45]Neurogenetic Clinic, Child Neurology Institute, Schneider Children's Medical Center of Israel, Petah Tiqvah, Israel. [46]Sackler School of Medicine, Tel-Aviv University, Ramat Aviv, Israel. [47]Zlotowski Center for Neuroscience, Ben-Gurion University, Beer-Sheva, Israel. [48]Pediatric Neurology Unit, Edmond and Lilly Safra Children's Hospital, Sheba Medical Center, Ramat-Gan, Israel. [49]Analytic and Translational Genetics Unit, Department of Medicine, Massachusetts General Hospital and Harvard Medical School, Boston, Massachusetts, USA. [50]Program in Medical and Population Genetics, Broad Institute of Harvard and MIT, Cambridge, Massachusetts, USA. [51]Stanley Center for Psychiatric Research, Broad Institute of Harvard and MIT, Cambridge, Massachusetts, USA. [52]Program in Genetics and Genomics, Biological and Biomedical Sciences, Harvard Medical School, Boston, Massachusetts, USA. [53]Centre for Neural Engineering, University of Melbourne, Melbourne, Victoria, Australia. [54]Wellcome Trust Sanger Institute, Wellcome Trust Genome Campus, Hinxton, UK. [55]Psychiatric and Neurodevelopmental Genetics Unit, Department of Psychiatry, Massachusetts General Hospital, Boston, Massachusetts, USA. [56]Department of Neurology, Massachusetts General Hospital, Boston, Massachusetts, USA. Correspondence should be addressed to A.-E.L. (anna-elina.lehesjoki@helsinki.fi).

ONLINE METHODS

Study subjects. The study cohort consisted of 84 unrelated individuals with a clinical presentation of PME, collected from multiple centers in Europe, North America, Asia and Australia over a 25-year period for molecular study, where a specific diagnosis had not hitherto been made. Seventy-three cases were of European origin, seven were of West Asian origin, three were of South Asian origin and one was of Chinese origin. The extent of previous molecular investigations varied; mutations in the *CSTB* gene had been excluded in all, 43 cases tested negative for mutations in *SCARB2* and 39 cases tested negative for mutations in *GOSR2*. A variable set of other genes was also screened for some cases. The study was approved by the institutional review board at the Helsinki University Central Hospital (Finland) and the human research ethics committees of Austin Health (Melbourne, Australia) and the University of South Australia (Adelaide, Australia). Informed consent for DNA analysis was obtained from study participants in line with local institutional review board requirements at the time of collection. Family members, when available, were recruited for segregation analysis, which was carried out using Sanger sequencing.

Seventy cases were sporadic. Three probands had either an affected parent or affected offspring. Ten probands had at least one affected sibling, and one proband had an affected cousin with known parental consanguinity. Fifteen of the cases were reported to be the result of a consanguineous union. On the basis of the inbreeding coefficients obtained with FEstim[56], the number of cases resulting from consanguinity was 18. No cryptic relatedness between cases (PIHAT > 0.05) was detected by PLINK[57] identity-by-descent (IBD) analysis.

Sanger sequencing was performed on a secondary cohort of 28 cases with PME or possible PME for the *KCNC1* recurrent mutation. These cases were excluded from our original cohort for exome sequencing owing to insufficient DNA or inadequate clinical data. Informed consent from study participants in the secondary cohort was obtained as described above for the exome sequencing cohort.

Exome sequencing. Exome sequencing was carried out at the Wellcome Trust Sanger Institute (Hinxton, UK). Genomic DNA (approximately 1 µg) extracted from peripheral blood for each sample was fragmented to an average size of 150 bp and subjected to DNA library creation using established Illumina paired-end protocols. Adaptor-ligated libraries were amplified and indexed via PCR. A portion of each library was used to create an equimolar pool comprising 4–8 indexed libraries. Each pool was hybridized to SureSelect Human All Exon 50Mb V3 RNA baits (Agilent Technologies), and sequence targets were captured and amplified in accordance with the manufacturer's recommendations. Enriched libraries were subjected to 75-base paired-end sequencing (HiSeq 2000, Illumina) following the manufacturer's instructions. Each pool of indexed samples was sequenced twice on two different flow cells.

Sequence read alignment and processing. Alignment of the sequenced DNA fragments to the human reference genome was performed using the Burrows-Wheeler Alignment Tool (BWA)[58]. The reference sequence used was the 1000 Genomes Project Phase II reference (hs37d5), which is based on GRCh37 and consists of chromosomes 1–22, X and Y, as well as the mitochondrial genome (rCRS mitochondrial sequence NC_012920), unlocalized and unplaced contigs, human herpesvirus 4 type 1 (NC_007605) and decoy sequences derived from HuRef, human BAC and fosmid clones and NA12878.

Duplicate reads were marked using the Picard toolkit. Sequence reads were further processed using Genome Analysis Toolkit (GATK) software (version 2.8.1)[59,60] on the basis of GATK best practices. Specifically, local realignment was performed around known insertion or deletion (indel) locations, and base quality scores were recalibrated.

Variant calling. SNVs and indels were called for all exomes jointly using the GATK HaplotypeCaller. Called variants with a quality score of >30 were accepted. Variant quality scores for the PME exomes were recalibrated jointly with the GATK VariantRecalibrator. HapMap 3.3 and the Omni 2.5M SNP chip array from the 1000 Genomes Project were used as truth site training resources in the variant quality score recalibration (VQSR) of SNVs. Mills and 1000 Genomes Gold Standard indels were used as truth sites in indel VQSR. A truth sensitivity cutoff of 99.0% was used for both SNVs and indels. Additional filtering was applied to exclude variant sites where >80% of the samples had <5× read depth. Individual variant calls with a read depth below 5× were excluded.

Variant filtering under recessive and dominant/*de novo* inheritance models. Considering the different possible inheritance patterns of the underlying mutations in the study subjects, we aimed to identify autosomal or sex-linked recessive and dominant (including *de novo*) mutations as well as pathogenic changes in the mitochondrial genome (**Fig. 1**). We considered coding variants with the following Variant Effect Predictor[61] (Ensembl release 75) annotated variant consequences based on Sequence Ontology nomenclature: missense variant, initiator codon variant, splice donor or acceptor variant, stop lost, stop gained, in-frame insertion or deletion (in-frame indels in tandem repeat regions[62] obtained from the UCSC Genome Browser[63] were excluded) and frameshift variant. If there were multiple Ensembl gene transcripts overlapping the variant site, the transcript having the most severe consequence annotation for the variant was selected while prioritizing Ensembl database canonical transcripts. Only variants within the genes included in the December 2013 version (release 15) of the Consensus CDS (CCDS) project, implemented in Ensembl release 75, were considered. To exclude likely benign amino acid changes, missense variants were considered only if two or more of the four *in silico* methods predicted the variant to be deleterious: CADD[64] (Phred-like scaled C score > 15, which is a suggested threshold for deleteriousness by the authors), PolyPhen-2 HumVar[65] (possibly damaging or probably damaging), SIFT[66] (deleterious) and MutationTaster[67] (disease causing; MutationTaster prediction scores were obtained using dbNSFP[68] and correspond to the converted score suggested by the authors). In rare cases, when not all of the four prediction methods could be applied, we accepted missense mutations predicted to be deleterious by at least 50% of the available methods. We also analyzed the exome data using only CADD to evaluate the deleteriousness of silent or noncoding mutations (**Supplementary Note**).

In recessive filtering, we included homozygous, hemizygous or compound heterozygous variants with allele frequencies of <1% in the 3 following variant databases: 1,092 exomes from the phase I release of the 1000 Genomes Project[69], 6,503 exomes from EVS in the NHLBI GO Exome Sequencing Project (version 0.0.25) and 3,268 Finnish exomes (Sequencing Initiative Suomi project, SISu; only autosomal SNVs, with epilepsy cases removed). Variants present in a homozygous or hemizygous state in any of the three variant databases were excluded. As we did not carry out exome sequencing of parental samples, we used three methods for phasing genotypes to facilitate the identification of compound heterozygous variants. First, physical phasing of SNV calls, based on the presence of heterozygous variants in the same sequencing reads, was performed using GATK ReadBackedPhasing. Because the ReadBackedPhasing method handles only SNVs, heterozygous indels present in the same sequencing reads were manually removed. Second, to detect rare variants segregating together in populations (likely to be inherited from only one parent), Beagle[70] was applied to phase genotypes using 1000 Genomes Project Phase I data as a reference. Third, we used genotype information from the 3,268 Finnish exomes to detect heterozygous variants likely to be on the same allele. After filtering the variant data using a recessive hypothesis, before taking advantage of the phasing information, we visualized the sequencing reads surrounding the variants that passed filtering using the Integrative Genomics Viewer[71] (IGV) to detect likely false positive calls residing mainly within segmental duplication regions where mapping of reads is more challenging. As a technical comparison set for variant visualization, we used 43 in-house exomes that had been processed in the same sequencing, read processing and variant calling pipelines as the exomes in this study. After excluding low-quality variants, we implemented the phasing information in the cleaned data and repeated the recessive filtering.

In the dominant/*de novo* filtering strategy, we assumed full penetrance of the mutations and, because the great majority of cases had disease onset before adulthood (10/84 cases had onset at 18 years or older, maximum onset age of 26 years), we included heterozygous variants absent from the three variant databases. Additionally, dbSNP Build 138 variants were excluded except those with clinical association in NCBI ClinVar. After applying the filtering criteria, we excluded low-quality variants on the basis of IGV visualization of sequencing reads as described for the filtering of recessive variants.

Analysis of filtered variant data under recessive and dominant/*de novo* strategies. Exome data were analyzed both for variants in genes previously associated with PME, epilepsy and/or neurodegenerative disorders and variants in new genes. The association of genes with mendelian diseases was annotated on the basis of the OMIM database[72]. Additionally, genes involved in monogenic forms of epilepsy and neurodegenerative disease were retrieved on the basis of the diagnostic panels developed by Lemke and colleagues[73]. Genes involved in PME were also retrieved from the literature.

To identify new recessive or dominant/*de novo* genetic causes, genes with variants surviving the filtering strategy were ranked on the basis of the number of PME cases with variants in the gene. Genes that are highly polymorphic in human populations and were thus likely to rank high in the data analysis only as a result of their high benign mutational load were given less priority if at least one of the following criteria was fulfilled: (i) the gene had a residual variation intolerance score (RVIS)[74] (estimating the tolerance of genes for functional variation) in the most tolerant tenth percentile (this criterion was used only in the dominant/*de novo* model) and (ii) the gene was identified as hyperpolymorphic by Fuentes Fajardo and colleagues[75]. Other measures used in the prioritization of candidate genes and variants were known disease association and the function (UniProt database[76] and the literature) and expression pattern (GTEx database[42] and the literature) of the gene.

Analysis of mitochondrial DNA variants. Because PME might also be caused by mutations in the mitochondrial genome[77], we analyzed the mtDNA for possible disease-associated mutations. Even though baits for mtDNA are not included in the SureSelect exome capture kit, we obtained an average of 32.7× sequencing coverage per sample in the mitochondrial genome, owing to the abundance of mtDNA in cells. We called mtDNA variants using the GATK UnifiedGenotyper. At sites for the most commonly reported mutations associated with diseases showing myoclonus as part of the clinical presentation, namely myoclonic epilepsy with ragged red fibers (MERRF) and mitochondrial encephalomyopathy, lactic acidosis and stroke-like episodes (MELAS), the average coverage was at least 24.8×. We searched for new mitochondrial mutations by excluding known mtDNA polymorphisms in the MITOMAP database. The same database was also used to obtain positions for known disease-associated mtDNA mutations.

Classification criteria for mutations in known as well as new disease-associated genes. We used a three-tier scale to classify mutations passing variant filtering in genes known to be associated with PME, epilepsy or neurodegenerative disease: (i) pathogenic, (ii) probably pathogenic and (iii) unlikely to be pathogenic. Classification criteria were as follows.

Pathogenic. The mutation was in a known PME-associated gene, i.e., where mutations cause a disease with PME as a key feature of the presentation, or in a gene known to be associated with epilepsy or neurodegenerative disease, had previously been reported as pathogenic and corresponded to a phenotype in the case that was compatible to those of previous cases. In addition, the mutation was required to map to a conserved domain where other pathogenic mutations had previously been reported. Segregation data, when available, had to comply with the expected inheritance pattern in the family, and the mode of inheritance had to concur with that for previously reported cases. If no segregation data were available, the corresponding phenotype had to present substantial overlap with those of previously reported cases, and, in the case of previously reported pathogenic compound heterozygous mutations, the mutations should not have occurred in *cis* in the original report.

Probably pathogenic. Either the mutation occurred in only one case in a previously established disease-related gene with phenotypic overlap with PME or occurred in a previously established neurological disease gene with little phenotypic overlap with PME and two or more cases had mutations in the gene. In addition, the mutation was required to map to a conserved domain where other pathogenic mutations had been reported previously. Segregation data for the mutation had to comply with the expected inheritance pattern in the family, and the mode of inheritance had to concur with that for previously reported cases.

Unlikely to be pathogenic. This category included mutations that did not fulfill the above criteria.

To consider new disease-associated genes as candidates for PME, we required them to harbor mutations in at least two cases in the recessive variant filtering strategy and in at least four cases in the dominant/*de novo* variant filtering strategy. The higher threshold in the dominant/*de novo* strategy was set to limit the number of candidates to a feasible level for follow-up, as exome variant data for the parents were not available for filtering inherited variants in data analysis.

Variant validation and segregation analysis. Candidate mutations in known and new disease-associated genes were confirmed and segregation of the variants was analyzed, when DNA from parents or siblings was available, by bidirectional Sanger sequencing (ABI BigDye 3.1, Applied Biosystems) on an ABI 3730xl DNA Analyzer. Primers (sequences available from the authors upon request) were designed with Primer-BLAST[78]. Sequences were analyzed using Sequencher (Gene Codes Corporation) and visualized using 4Peaks (Nucleobytes). Evaluation of the quality of the sequence reads over the recurrent c.959G>A mutation in *KCNC1* is described in the **Supplementary Note**.

Parental testing of the cases with the c.959G>A mutation in *KCNC1*. Parental testing was carried out for five cases (those with a sufficient amount of parental DNA available) with the *de novo* c.959G>A mutation in *KCNC1* to exclude false paternity and inadvertent sample substitution. Biparental testing was performed using 12 highly polymorphic microsatellite markers: D3S3680, D4S418, D6S289, D7S2560, D8S281, D13S175, D13S221, D15S117, D19S1150, DXS1113, DXS1036 and DXS7423. PCR was performed using the Qiagen Multiplex PCR kit according to the manufacturer's instructions. The reverse primer of each pair was labeled with either HEX or FAM. Products were analyzed on an ABI 3131 Genetic Analyzer.

Analysis of parental mosaicism for the c.959G>A mutation in *KCNC1* in the family of PME84-1. The PCR product corresponding to exon 2 of *KCNC1* was amplified using the same primers and conditions as for sequencing, and 10 µl of the PCR reaction was digested with 2 U HpyCH4V (New England BioLabs) for 2 h at 37 °C under the conditions recommended by the manufacturer. Fragments were visualized by electrophoresis of 10 µl of the digest on a 2% agarose gel in TBE buffer. Gels were stained with RedSafe (INtRON Biotechnology). PCR and digestion were performed in duplicate.

Evaluation of the expected rate of mutations encoding arginine-to-histidine changes in the S4 segment of K_V3.1. The expected rates for the four possible mutations encoding arginine-to-histidine changes (CGC>CAC) in the voltage-sensing arginine residues of the K_V3.1 S4 segment (p.Arg311His, p.Arg314His, p.Arg317His and p.Arg320His; **Fig. 2b**,**c**) were established using a recently developed statistical framework[10], which takes into account both the local sequence context of a mutation site and regional factors such as divergence between humans and macaques.

Functional analysis of the p.Arg320His substitution in K_V3.1. *Mutagenesis and RNA preparation.* We used the QuikChange kit (Stratagene) to engineer the missense mutation c.959G>A (p.Arg320His) into human *KCNC1* cDNA (NM_004976; this construct corresponds to the K_V3.1a isoform (511 amino acids), which has a shorter cytoplasmic C-terminal domain but identical biophysical properties in comparison to the longer K_V3.1b (585 amino acids) isoform[79]) cloned in a pCMV-Entry vector obtained from OriGene Technologies. This clone encodes a C-terminal Myc-DDK tag. Introduction of the mutation was confirmed and the presence of additional mutations was excluded by Sanger sequencing. Primer sequences are available upon request. cRNA was prepared using the T7 mMessage mMachine kit from Ambion.

Oocyte preparation and injection. The use of animals and all experimental procedures were approved by local authorities (Regierungspraesidium Tübingen, Tübingen, Germany). Extracted ovary pieces (*X. laevis*) obtained from the Institute of Physiology I, Tübingen, were treated with collagenase (1 mg/ml type CLS II collagenase, Biochrom) in OR-2 solution (82.5 mM NaCl, 2.5 mM KCl, 1 mM $MgCl_2$ and 5 mM HEPES, pH 7.6), washed thoroughly and stored at 16 °C in Barth solution (88 mM NaCl, 2.4 mM $NaHCO_3$, 1 mM

doi:10.1038/ng.3144

KCl, 0.33 mM $Ca(NO_3)_2$, 0.41 mM $CaCl_2$, 0.82 mM $MgSO_4$ and 5 mM Tris-HCl, brought to pH 7.4 with NaOH) supplemented with 50 µg/ml gentamicin (Biochrom). Equal volumes (50 nl) of cRNA with the concentration adjusted to 2 µg/µl were injected into the same batch of oocytes plated in 96-well plates using Robooinject (Multi Channel Systems). Recordings were performed in parallel at days 2–3 after injection. Amplitudes of interest for all currents recorded on the same day were normalized to the mean value obtained for wild-type $K_V3.1$ on that day so that the normalized data from different experiments could be pooled. Sample sizes were not predetermined.

Automated oocyte two-microelectrode voltage clamp. Potassium ion currents in oocytes were recorded at room temperature (20–22 °C) on Roboocyte2 (Multi Channel Systems) using prepulled and prepositioned intracellular glass microelectrodes with a resistance of 0.3–1 MΩ when filled with a solution of 1 M KCl and 1.5 M potassium acetate. The bath solution was ND96 (93.5 mM NaCl, 2 mM KCl, 1.8 mM $CaCl_2$, 2 mM $MgCl_2$ and 5 mM HEPES, pH 7.5). Currents were sampled at 5-kHz intervals. For the analysis of channel activation, we kept cells at the holding potential of –90 mV and used 0.5-s depolarizing steps (Δ10 mV) from –60 mV to +60 mV, followed by a step to –90 mV for 0.5 s to analyze tail currents.

Data analysis. Voltage clamp recordings were analyzed using Roboocyte2+ (Multi Channel Systems), Clampfit (pClamp 8.2, Axon Instruments), Excel (Microsoft) and Origin (OriginLab Corp.) software. The voltage dependence of channel activation was determined from tail current amplitudes recorded at –90 mV. A Boltzmann function was fit to each current-voltage relationship, $I(V) = I_{max}/(1 + \exp((V - V_{0.5})/k)) + C$, where I_{max} is the maximum tail current amplitude at test potential V, $V_{0.5}$ is the half-maximal activation potential, k is a slope factor reflecting the characteristics of voltage-dependent channel gating and C is a constant. Maximum current amplitudes were compared at the end of a 0.5-s test pulse to +60 mV. All data are shown as mean values ± s.e.m. Statistical analysis was performed with GraphPad software, and significant differences ($P < 0.05$) were determined using the Student's t test or Mann-Whitney U test.

Protein blotting. For protein blots, injected *Xenopus* oocytes were lysed in buffer containing 20 mM Tris, 100 mM NaCl, 1 mM EDTA, 0.5% Triton X-100 and 10% glycerol with Complete protease inhibitors (Roche). After we determined protein concentrations (BCA system, Thermo Fisher Scientific), 20 µg of protein for each sample was separated by SDS-PAGE on 8% polyacrylamide gels. The proteins were transferred onto nitrocellulose membrane (Whatman, GE Healthcare Europe), and protein blotting was performed using a mouse monoclonal antibody to the DDK tag (1:1,500 dilution; OriGene Technologies, TA50011). Chemiluminescence detection was carried out according to the manufacturer's protocol (ECL Western Detection Kit, Amersham Pharmacia Biotech Europe). Actin was used as a loading control.

56. Leutenegger, A.-L. *et al.* Estimation of the inbreeding coefficient through use of genomic data. *Am. J. Hum. Genet.* **73**, 516–523 (2003).
57. Purcell, S. *et al.* PLINK: a tool set for whole-genome association and population-based linkage analyses. *Am. J. Hum. Genet.* **81**, 559–575 (2007).
58. Li, H. & Durbin, R. Fast and accurate short read alignment with Burrows-Wheeler transform. *Bioinformatics* **25**, 1754–1760 (2009).
59. McKenna, A. *et al.* The Genome Analysis Toolkit: a MapReduce framework for analyzing next-generation DNA sequencing data. *Genome Res.* **20**, 1297–1303 (2010).
60. DePristo, M.A. *et al.* A framework for variation discovery and genotyping using next-generation DNA sequencing data. *Nat. Genet.* **43**, 491–498 (2011).
61. McLaren, W. *et al.* Deriving the consequences of genomic variants with the Ensembl API and SNP Effect Predictor. *Bioinformatics* **26**, 2069–2070 (2010).
62. Benson, G. Tandem repeats finder: a program to analyze DNA sequences. *Nucleic Acids Res.* **27**, 573–580 (1999).
63. Kent, W.J. *et al.* The Human Genome Browser at UCSC. *Genome Res.* **12**, 996–1006 (2002).
64. Kircher, M. *et al.* A general framework for estimating the relative pathogenicity of human genetic variants. *Nat. Genet.* **46**, 310–315 (2014).
65. Adzhubei, I.A. *et al.* A method and server for predicting damaging missense mutations. *Nat. Methods* **7**, 248–249 (2010).
66. Kumar, P., Henikoff, S. & Ng, P.C. Predicting the effects of coding non-synonymous variants on protein function using the SIFT algorithm. *Nat. Protoc.* **4**, 1073–1081 (2009).
67. Schwarz, J.M., Rodelsperger, C., Schuelke, M. & Seelow, D. MutationTaster evaluates disease-causing potential of sequence alterations. *Nat. Methods* **7**, 575–576 (2010).
68. Liu, X., Jian, X. & Boerwinkle, E. dbNSFP v2.0: a database of human non-synonymous SNVs and their functional predictions and annotations. *Hum. Mutat.* **34**, E2393–E2402 (2013).
69. 1000 Genomes Project Consortium. An integrated map of genetic variation from 1,092 human genomes. *Nature* **491**, 56–65 (2012).
70. Browning, B.L. & Browning, S.R. Improving the accuracy and efficiency of identity-by-descent detection in population data. *Genetics* **194**, 459–471 (2013).
71. Robinson, J.T. *et al.* Integrative genomics viewer. *Nat. Biotechnol.* **29**, 24–26 (2011).
72. Hamosh, A., Scott, A.F., Amberger, J.S., Bocchini, C.A. & McKusick, V.A. Online Mendelian Inheritance in Man (OMIM), a knowledgebase of human genes and genetic disorders. *Nucleic Acids Res.* **33**, D514–D517 (2005).
73. Lemke, J.R. *et al.* Targeted next generation sequencing as a diagnostic tool in epileptic disorders. *Epilepsia* **53**, 1387–1398 (2012).
74. Petrovski, S., Wang, Q., Heinzen, E.L., Allen, A.S. & Goldstein, D.B. Genic intolerance to functional variation and the interpretation of personal genomes. *PLoS Genet.* **9**, e1003709 (2013).
75. Fuentes Fajardo, K.V. *et al.* Detecting false-positive signals in exome sequencing. *Hum. Mutat.* **33**, 609–613 (2012).
76. UniProt Consortium. Activities at the Universal Protein Resource (UniProt). *Nucleic Acids Res.* **42**, D191–D198 (2014).
77. Shoffner, J.M. *et al.* Myoclonic epilepsy and ragged-red fiber disease (MERRF) is associated with a mitochondrial DNA $tRNA^{Lys}$ mutation. *Cell* **61**, 931–937 (1990).
78. Ye, J. *et al.* Primer-BLAST: a tool to design target-specific primers for polymerase chain reaction. *BMC Bioinformatics* **13**, 134 (2012).
79. Gu, Y., Barry, J., McDougel, R., Terman, D. & Gu, C. Alternative splicing regulates $K_V3.1$ polarized targeting to adjust maximal spiking frequency. *J. Biol. Chem.* **287**, 1755–1769 (2012).